Bioconjugate Chemistry

pubs.acs.org/bc

Article

Delivery of Cas9/sgRNA Ribonucleoprotein Complexes via Hydroxystearyl Oligoamino Amides

Jasmin Kuhn, Yi Lin, Ana Krhac Levacic, Nader Al Danaf, Lun Peng, Miriam Höhn, Don C. Lamb, Ernst Wagner, and Ulrich Lächelt*

Cite This: *Bioconjugate Chem.* 2020, 31, 729–742

Read Online

ACCESS | Metrics & More | Article Recommendations | Supporting Information

ABSTRACT: The programmable endonuclease activity and simple usage of CRISPR/Cas9 have revolutionized the field of genome editing. The binding of single guide RNA (sgRNA) by the Cas9 protein results in the formation of negatively charged ribonucleoprotein (RNP) complexes. The presence of this functional complex inside cells is imperative for the intended specific genome modifications. The direct intracellular delivery of Cas9/sgRNA RNP complexes is of great advantage. In this work, a compound library of sequence-defined oligo(ethylenamino) amides containing structural motifs for stable nanoparticle formation, cellular uptake, and endosomal release was used for the screening and development of suitable Cas9 RNP delivery vehicles. Lipid-containing oligoaminoamides (lipo-OAAs) were identified as the most efficient carriers for intracellular Cas9/sgRNA delivery and gene disruption. Fluorescence correlation spectroscopy measurements indicated that the lipo-OAAs only interact with sgRNA-loaded Cas9 protein, which suggests exclusive ionic interaction with the negatively charged RNPs. The type of contained fatty acid turned out to have a critical impact on the knock out efficiency: the presence of one hydroxy group in the fatty acid dramatically changes the properties and performance of the resulting Cas9/sgRNA lipo-OAA complexes. The lipo-OAA-containing hydroxy-stearic acid (OHSteA) was superior to the analogues with saturated or unsaturated fatty acids without hydroxylation; it formed smaller and more defined nanoparticles with Cas9/sgRNA and improved the cellular uptake and endosomal release, which altogether resulted in an increased nuclear association and the highest gene knock out levels. The efficient and adaptable delivery platform has high potential for the future development of therapeutics based on precise genome modifications.

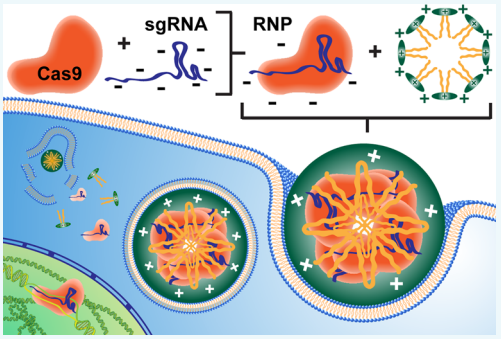

INTRODUCTION

Protein therapeutics have emerged as a major new class of biopharmaceuticals, since the discovery and approval of the first recombinant protein drug.[1,2] This class of drugs, which includes hormones, antibodies, cytokines, growth factors, enzymes, as well as bone and blood-related agents,[1,3,4] exhibits an enormous therapeutic potential due to its involvement in various biochemical processes and its high specificity, tolerability, and safety.[5] CRISPR (clustered, regularly interspaced, short palindromic repeats) Cas (CRISPR-associated) is an adaptable DNA cleavage system found in bacteria[6,7] and has been utilized as an efficient RNA-guided genome-editing tool in numerous species[8−10] as well as in human cells.[11,12] The target sequence of the programmable nuclease Cas9 is controlled by a guide RNA (a combination of crRNA and tracrRNA) or a single guide RNA (sgRNA).[7] For efficient genome editing, a successful intracellular delivery of the CRISPR/Cas9 components is essential. So far, the most common strategy is based on the delivery of the CRISPR/Cas9 encoding DNA sequences or in vitro transcribed RNA molecules.[13] However, the direct delivery of the Cas9 protein complexed with sgRNA has several advantages over the delivery of the corresponding nucleic acid precursors, as the ribonucleoprotein (RNP) complex is immediately functional without the requirement of transcription and translation. Furthermore, there is no risk of spontaneous genome integration, and timely degradation reduces potential off-target effects.[14] Because nucleic acids and proteins are susceptible to enzymatic degradation, the incorporation into a carrier system can increase their stability.[15,16] In addition, the poor membrane permeability impedes transport of Cas9/sgRNA RNPs to the intracellular target site and requires the development of suitable delivery vehicles.[17] Different nonviral delivery technologies have evolved for the direct delivery of the RNP complexes,[18] including cell-penetrating peptides,[19] DNA nanoclews,[20] gold nanoparticles,[21,22] polymeric systems,[23−25] as well as black phosphorus nanosheets,[26] hydrogels,[27] or lipid nanoparticles.[28,29] Nonetheless, a requirement of better carriers

Received: December 18, 2019
Revised: January 20, 2020
Published: January 22, 2020

https://dx.doi.org/10.1021/acs.bioconjchem.9b00853
Bioconjugate Chem. 2020, 31, 729–742

for stable RNP packaging, high cellular uptake, efficient endosomal escape, and nuclear entry while preserving biological activity remains.

Sequence-defined oligo(ethylenamino) amides (OAAs) based on artificial oligoamino acids and solid-phase synthesis have recently been developed as a platform for the delivery of nucleic acids,[30] proteins,[16] and drugs.[31] They combine the advantages of aminoethylene-based polymers[32,33] with the chemical precision of peptides and enable cargo-specific optimization.[34] OAAs with a favorable stability, biocompatibility, and toxicity profile have been generated.[30,35] In this study, lipo-OAAs were established as a new delivery platform for codelivery of the Cas9 protein and sgRNA. Different architectures were screened to identify favorable structural motifs and the most suitable reagents. Here, the artificial oligoamino acids were intended to complex the negatively charged RNP complexes and facilitate their cellular delivery. Additional cysteines (C) and hydrophobic motifs, like the tyrosine (Y) tripeptide, have been shown to improve nanoparticle stability in the context of other delivery purposes.[36,37] Fatty acids can enable efficient intracellular delivery by promoting membrane interaction and endosome disruption.[38−40]

RESULTS AND DISCUSSION

Lead Structure Identification. To assess the general potential of OAAs for Cas9/sgRNA RNP delivery, a first library screen was conducted. Recombinant Cas9 was produced by bacterial expression, sgRNA was synthesized by in vitro transcription, and RNP functionality was assessed by an in vitro cleavage assay (Figure S1). Sequence-defined OAAs with different architectures and structural motifs were selected, which, in previous studies, showed efficient intracellular delivery of other cargos such as small interfering RNA (siRNA), plasmid DNA (pDNA), and proteins.[30,37,41,42] The GFP reporter gene was used as a read-out to assess the knock out efficiency and thereby identify the best performing structures. For a sensitive detection of promising architectures in the initial screen, Neuro2a eGFP-Luc cells were treated with Cas9/sgRNA RNP formulations for 4 h without serum. Subsequently, serum was added, and cells were incubated for an additional 44 h. All samples were analyzed by flow cytometry 3−4 days after cell treatment. As expected, the bare RNP complexes did not induce substantial GFP knock out (Figure S2). Commercially available Lipofectamine 3000 (LF 3) achieved a reporter gene knock out of approximately 11% at higher concentrations, while succinylated polyethylenimine (PEI-Suc)[43] increased knock out levels to 15%. Sequence-defined OAAs with a comb-like architecture, which initially were designed as efficient pDNA delivery agents,[41] did not induce a significant knock out of GFP with Cas9/sgRNA. In contrast, branched 3- and 4-arm OAAs exhibited distinct Cas9/sgRNA delivery efficiency. In the case of 3-arm OAAs, the introduction of hydrophobic tyrosine tripeptide motifs strongly improved the GFP knock out efficiency from 2% (Stp-H-C) to 18% (Stp-H-Y3-C). A 4-arm OAA (Sph-H-C) based on the artificial oligoamino acid succinyl-pentaethylene hexamine (Sph) mediated 23% GFP knock out. A substitution of Sph with the shorter oligoamino acid glutaryl-triethylene tetramine (Gtt-H-C) eliminated the delivery efficiency completely, which demonstrates the critical impact of slight structural variations and the need for optimal composition. The highest Cas9/sgRNA delivery potency and approximately 28% GFP knock out efficiency were observed with a lipid-modified T-shape structure (T-OleA) containing the cationizable oligoamino acid succinyl-tetraethylene pentamine (Stp), oleic acid, and stabilizing tyrosine trimers.[36] The same oligomer did not induce any reduction of GFP expression with Cas9/cgRNA RNP containing a control guide RNA (cgRNA) without a specific target in the genome, which confirms the sequence-specific GFP knock out.

Lipid Variation. The initial library screen identified the T-shape oligomer T-OleA as the best-performing structure for the Cas9/sgRNA RNP delivery (Figure S2). The fatty acids used in the delivery system are suggested to boost intracellular delivery by hydrophobic nanoparticle stabilization as well as endosomal membrane interaction and release.[38,44,45] On the basis of the promising results obtained with T-OleA, which contains the unsaturated C18 fatty acid oleic acid (OleA), different T-shape lipo-OAAs with fatty acid variations were screened under the biologically more relevant conditions in the presence of serum (Figure 1). We recently reported that the

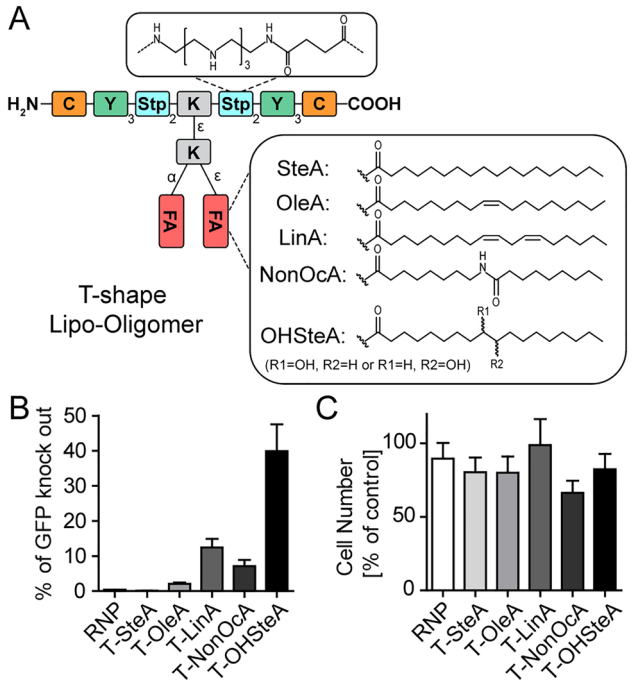

Figure 1. Lipid variation. (A) A schematic illustration of T-shape OAAs with different fatty acids (FA). SteA, stearic acid; OleA, oleic acid; LinA, linoleic acid; NonOcA, nonanamidooctanoic acid; OHSteA, hydroxystearic acid; Stp, succinyl-tetraethylene pentamine. (B) GFP knock out efficiency determined by flow cytometry and (C) cell number of Neuro2a eGFP-Luc cells 3−4 d after the 48 h treatment with 75 nM RNP lipo-nanoparticles (with a nitrogen/phosphate N/P ratio of 24) targeting the eGFP gene. Cells were normalized to the control measurements with HBG buffer treated cells. RNP complex without lipo-OAA served as negative control. Data are presented as mean ± SD (n = 3).

degree of saturation of the fatty acid moiety critically impacts the delivery of phosphorodiamidate morpholino oligomers (PMOs).[40] Analogues of T-OleA containing saturated stearic acid, bis-unsaturated linoleic acid (LinA), 8-nonanamidooctanoic acid (NonOcA), and hydroxystearic acid (OHSteA) instead of oleic acid were synthesized (Figure 1A). To determine the influence of the fatty acid variation, Neuro2a eGFP-Luc cells were incubated with Cas9/sgRNA RNP

https://dx.doi.org/10.1021/acs.bioconjchem.9b00853
Bioconjugate Chem. 2020, 31, 729−742

formulations for 48 h in serum-containing medium (Figure 1B). As expected, the bare RNP complexes did not induce GFP knock out. In the presence of serum, which represents more challenging conditions as compared to the initial library screen, neither saturated T-SteA nor the monounsaturated T-OleA resulted in significant GFP knock out. In contrast, bis-unsaturated T-LinA and amide-containing T-NonOcA increased the GFP knock out efficiency to around 12% or 7%, respectively. Notably, the hydroxylated T-OHSteA mediated the highest GFP knock out with an efficiency of 40% after the single Cas9/sgRNA treatment. The cell number after the treatments with the lipo-nanoparticles was determined as a measure for nanoparticle toxicity (Figure 1C). All lipo-nanoparticles were generally well tolerated with T-NonOcA exhibiting the highest decrease in cell number.

Nanoparticle Formation. The lipo-nanoparticles that were formed from T-shape lipo-OAAs containing the different lipid variations and the RNP complex were further characterized in terms of their physicochemical properties, because they can significantly impact the in vitro and in vivo characteristics of a carrier system.[46,47] The nanoparticle size, polydispersity, and zeta potential were determined by DLS (Figure 2A–C). Lipo-nanoparticles containing Cas9/sgRNA and the saturated (T-SteA), mono- (T-OleA), and bis-unsaturated fatty acids (T-LinA) or the amide-lipid (T-NonOcA) displayed hydrodynamic diameter of 247–293 nm, whereas the more hydrophilic hydroxylated T-OHSteA analogue produced significantly smaller nanoparticles with a *z*-average of 168 nm (Figure 2A). The polydispersity index (PDI) as a measure for the homogeneity of the particle population (Figure 2B) also suggested a more homogeneous nanoparticle formation with T-OHSteA (PDI 0.24) as compared to the other four oligomers (PDI 0.45–0.56). The zeta potential of all lipo-nanoparticles ranged from +15 to +18 mV (Figure 2C), suggesting positive surface charges, which are beneficial for cellular uptake via electrostatic interactions.[48]

In view of addressing the interaction between sgRNA and Cas9, the RNP complex formation, and the RNP interaction with the T-OHSteA oligomer, fluorescence correlation spectroscopy (FCS) was used (Figure 2D–F). FCS records and analyzes the intensity fluctuations through a small (~femtoliter) observation volume, caused by the diffusion of fluorescent particles in and out of this observation volume. From the temporal autocorrelation function (ACF) of the signal, a slower diffusion coefficient due to the formation of complexes causes a shift in the temporal ACF to slower time scales.[49−51] The diffusion of the single-labeled ATTO647N-Cas9 (18.2 $\mu m^2/s$) and ATTO488-sgRNA (56.0 $\mu m^2/s$) corresponds to their individual molecular weights and confirms the presence of a monomolecular species in solution (Figure 2D and E, light blue curves) (Tables S3 and S4). Addition of the positively charged oligomer T-OHSteA to the Cas9 protein does not mediate a shift toward higher time lag τ, indicating the absence of strong interactions between the two components (Figure 2D, orange curve). In contrast, the addition of T-OHSteA to sgRNA shows a strong shift of the autocorrelation function toward a higher time lag τ due to the formation of an RNA polyplex (Figure 2E, orange curve). The appearance of a slowly diffusing component (4.02 $\mu m^2/s$) is a further indication of the RNA polyplex formation (Table S3). Similarly, the mixture of sgRNA and Cas9 protein shows a species with slower diffusion in both channels (~1.5 $\mu m^2/s$), suggesting the formation of Cas9/sgRNA RNP complexes

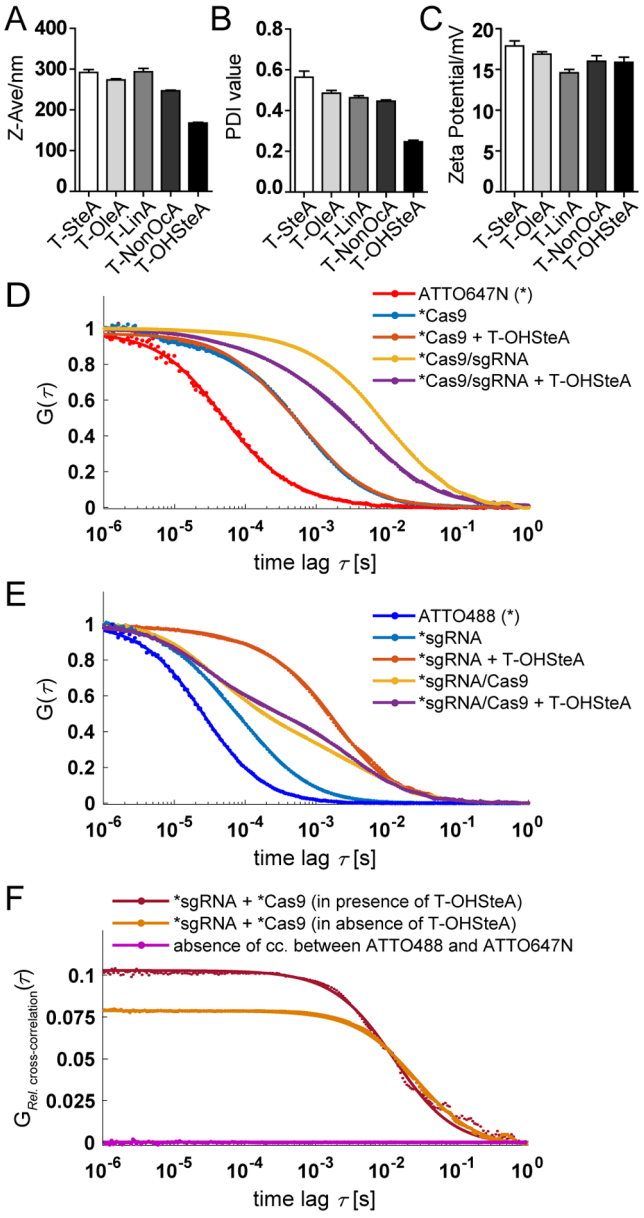

Figure 2. Cas9/sgRNA RNP nanoparticle formation characterized by dynamic light scattering (A–C) and fluorescence (cross-) correlation spectroscopy (D–F). (A) The hydrodynamic particle size (*z*-average) in nanometer, (B) polydispersity index (PDI), and (C) zeta potential in millivolt of 75 nM Cas9/sgRNA solutions complexed with different lipo-OAAs at an N/P ratio of 24. Particles were formed in HBG, and three technical replicas were measured. (D) The autocorrelation function (ACF) of 100 nM ATTO647N-Cas9 showing its interaction with 100 nM ATTO488-sgRNA and 19 μM T-OHSteA (corresponding to an N/P ratio of 24). The ACF of ATTO647N alone is shown as a reference for a freely diffusing fluorophore. Note that the orange curve is largely overlapping the blue curve. The asterisk (*) indicates the fluorescent species that is detected (red channel). (E) The ACF of 100 nM ATTO488-sgRNA showing its interaction with 100 nM ATTO647N-Cas9 and 19 μM T-OHSteA (corresponding to an N/P ratio of 24). The ACF of ATTO488 alone is shown as a reference for a freely diffusing fluorophore. The slower decay of the ACFs represented by the shift toward higher time lag τ indicates a slower diffusion and an increase in the hydrodynamic size due to complex formation. The asterisk (*) indicates the fluorescent species that is detected (green channel). (F) The relative cross-correlation (obtained by the division of the CCF amplitude by the ACF amplitude of the ATTO647N-Cas9) between 100 nM ATTO647N-

https://dx.doi.org/10.1021/acs.bioconjchem.9b00853
Bioconjugate Chem. 2020, 31, 729–742

Figure 2. continued

Cas9 and 100 nM ATTO488-sgRNA in the presence (red) or absence (orange) of 19 μM T-OHSteA (corresponding to an N/P ratio of 24). A mixture of ATTO647N and ATTO488 served as a reference showing the absence of any cross-correlation between the freely diffusing fluorophores (pink curve). The lines represent the obtained fit for the data points represented as dots. The asterisk (*) indicates the fluorescent species that are detected (red and green channels).

(Figure 2D and E, yellow curves) (Tables S3 and S4). Additionally, we performed fluorescence cross-correlation spectroscopy (FCCS) experiments, a dual-color extension of standard FCS.[52,53] Here, the temporal cross-correlation functions (CCFs) between the detection channels for the two fluorescently labeled ATTO647N-Cas9 and ATTO488-sgRNA proteins were analyzed. In FCCS, a cross-correlation signal is only present in the case of concerted motion of the different labels, such as after formation of RNP complexes. Thus, not only is the temporal decay of the CCF changed upon binding, but also the amplitude, making it much more sensitive as compared to standard FCS.[52] The interaction of Cas9 and sgRNA and thus RNP formation are confirmed by the cross-correlation of the two differently labeled components (Figure 2F, orange curve). The addition of T-OHSteA to Cas9/sgRNA RNPs results in a slightly faster diffusion coefficient, suggesting the reassembly or compaction of the RNP complexes, upon the addition of the highly positive oligomers (Figure 2D and E, purple curve). This compaction is better observable in the CCF (Figure 2F, absence vs presence of T-OHSteA) where the diffusion coefficients of the RNP complex in the presence (~0.5 $\mu m^2/s$) and in the absence (~1 $\mu m^2/s$) of the T-OHSteA show the compaction resulting in an increase in mobility by a factor of 2. Importantly, the addition of the cationic T-OHSteA does not appear to disrupt the RNPs by detachment of sgRNA from the Cas9 protein, because the relative cross-correlation amplitude does not decrease but actually increases slightly upon addition of the oligomer (Figure 2F).

Cellular Delivery Pathway. The intracellular target site of Cas9/sgRNA RNPs is inside the nucleus. Critical bottle-necks within the delivery pathway are the cellular uptake, endosomal

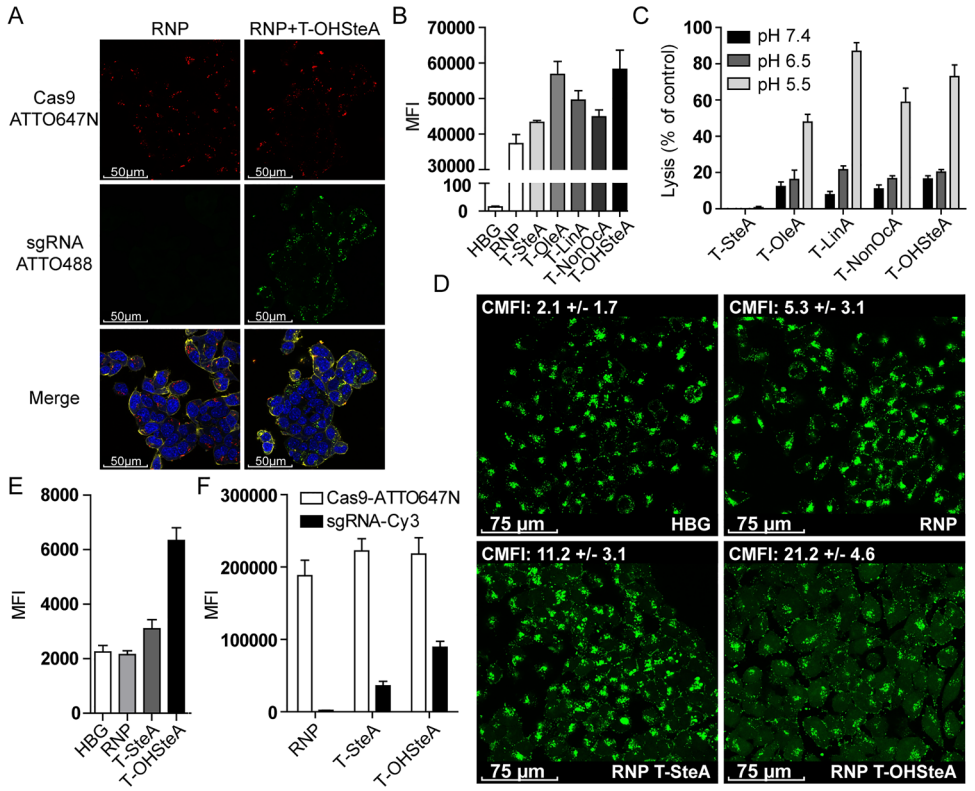

Figure 3. Effect of Cas9/sgRNA RNP formulations on cellular delivery barriers: cellular uptake (A,B), membrane interaction and endosomal escape (C–E), and nuclear association (F). (A) CLSM images of Neuro2a cells treated for 4 h with 75 nM Cas9/sgRNA RNPs (Cas9:sgRNA 1:1, 20% ATTO647N-labeled Cas9 protein, 20% ATTO488-labeled sgRNA) with (right) or without (left) encapsulation into T-OHSteA at an N/P ratio of 24. Additional data of the full set of all RNP lipo-nanoparticles can be found in Figure S3. (B) Cellular ATTO647N-Cas9 fluorescence intensity determined by flow cytometry after 4 h incubation with 75 nM RNP formulations (median fluorescence intensity, MFI, $n = 3$). (C) Erythrocyte leakage assays by photometrical determination of hemoglobin that was released from 3.75×10^6 erythrocytes after 60 min incubation with 2.5 μM lipo-OAA at pH 7.4, 6.5, or 5.5. Values were normalized to positive control samples treated with 1% (v/v) Triton X-100 (100% lysis). Data are presented as mean ± SD ($n = 4$). (D) CLSM images measuring the amount of endosomal calcein release of Neuro2a cells after 4 h incubation with 0.4 mg/mL calcein for different formulations: HBG only (top, left), 75 nM RNPs (top, right), 75 nM RNP T-SteA (bottom, left), or 75 nM RNP T-OHSteA (bottom, right). Cytosolic mean fluorescence (CMFI) was determined by ImageJ (Figure S4). Data are presented as mean ± SD ($n = 10$). (E) Cellular calcein fluorescence intensity determined by flow cytometry (median fluorescence intensity, MFI, $n = 3$). (F) Nuclear association of Cas9-ATTO647N and sgRNA-Cy3 (median fluorescence intensity, MFI, $n = 3$) determined by flow cytometry on isolated nuclei. Neuro2a cells were incubated for 24 h with 75 nM RNP complexes without (RNP) or with lipo-OAA formulation (T-SteA, T-OHSteA). Cells were permeabilized by 40 μg/mL digitonin, and nuclei were isolated by centrifugation.

https://dx.doi.org/10.1021/acs.bioconjchem.9b00853
Bioconjugate Chem. 2020, 31, 729–742

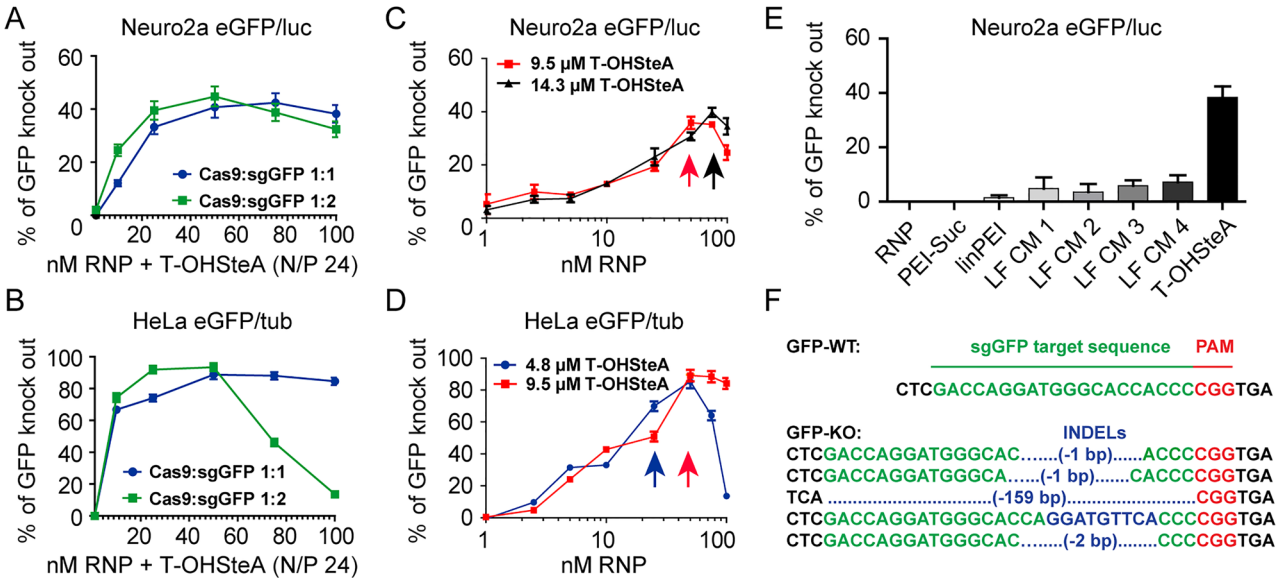

Figure 4. Dose-titration and characterization of RNP T-OHSteA formulations. (A,B) Dose-titration experiments in Neuro2a eGFP-Luc (A) or HeLa GFP-Tub (B) cells treated with 1−100 nM Cas9/sgRNA RNP complex at a 1:1 (blue) or 1:2 (green) ratio formulated with T-OHSteA at an N/P ratio of 24. (C) The N/P ratio was varied in Neuro2a eGFP-Luc cells by keeping the T-OHSteA concentration constant (red curve, 9.5 μM; black curve, 14.3 μM) and varying the amount of RNP complexes (in nM) at a 1:1 ratio. Arrows of the same color indicate an N/P ratio of 24. (D) N/P variation experiments in HeLa GFP-Tub cells where the T-OHSteA concentration was held constant (blue curve, 4.8 μM; red curve, 9.5 μM) and the amount of RNP complexes was varied at a 1:1 ratio. Arrows of the same color indicate an N/P ratio of 24. (E) Comparison of RNP T-OHSteA formulations with established transfection reagents in terms of knock out efficiency. RNP complex without carrier served as a negative control. Established transfection reagents included succinylated polyethylenimine (PEI-Suc) at a w/w ratio of 4 and linear polyethylenimine (linPEI) at a w/w ratio of 0.8 of polymer to sgRNA. Lipofectamine CRISPRMAX (LF CM) was tested at three different concentrations and with two different mixing procedures. LF CM 1 (6 nM RNPs) and 2 (15 nM RNPs) and 3 (75 nM RNPs) were prepared as recommended by the manufacturer. LF CM 4 (75 nM RNPs) as well as T-OHSteA (75 nM RNPs) were mixed according to the protocol for RNP lipo-OAA formulation. All data points indicate the % knock out efficiency 3−4 d after 48 h treatment in the presence of 10% FBS. The % of GFP knock out was normalized to HBG buffer treated cells. Data are presented as mean ± SD (n = 3). (F) Sequencing of monoclonal GFP knock out cells. The green sequence indicates the sgRNA target sequence in the eGFP gene next to the protospacer adjacent motive (PAM) sequence in red. Insertions and deletions caused by the DNA repair mechanisms after the Cas9-induced double-strand break are highlighted in blue.

release, and nuclear entry. The ability of RNP lipo-OAA formulations to overcome the separate delivery barriers was assessed in a series of experiments (Figure 3). The cellular uptake of the Cas9/sgRNA complex formulations into Neuro2a cells was visualized by confocal laser scanning microscopy (CLSM, Figure 3A). To investigate the uptake of both RNP components individually, the Cas9 protein and the sgRNA were labeled with fluorescent dyes ATTO647N and ATTO488, respectively. While cellular internalization of the Cas9 protein (top images, red channel) was observed for both formulated (RNP+T-OHSteA) as well as bare RNP complexes (RNP), intracellular sgRNA was only detected in combination with the lipo-OAA (middle images, green channel). A possible explanation for this observation is the stabilization and protection of single-stranded RNA by complexation and encapsulation in the carrier system.[15] Importantly, these data show that only the lipo-nanoparticles mediate codelivery of both functional RNP components, which are essential for genome editing activity. The lipid modification of the T-shape lipo-OAA turned out to have a major impact on GFP knock out efficiency (Figure 1).

To investigate a possible explanation for the importance of the lipid modification, lipo-nanoparticle uptake into Neuro2a cells was quantified by flow cytometry in a comparative study (Figure 3B). The monounsaturated T-OleA and hydroxylated T-OHSteA mediated the highest levels of cellular internalization, while all other screened compounds were inferior. Because no distinct difference between the T-OleA and T-OHSteA was observed, the superiority of T-OHSteA in terms of GFP reporter gene knock out efficiency cannot be explained by higher cellular uptake. Inadequate endosomal escape has often been identified as a key bottleneck in cellular delivery of biomolecules.[15,54,55] Because the conducted cellular uptake study does not identify the intracellular localization and, in particular, does not differentiate between the endolysosomal or cytosolic compartment, the advantage of T-OHSteA lipid nanoparticles might be related to a superior endosomal release. The amphiphilic character of the lipid-modified cationic oligomer provides the potential of lytic membrane interactions. Previous nucleic acids studies have shown that unsaturated fatty acids can enhance pH-dependent membrane lysis and thereby endosomal escape.[36,37,56] Erythrocyte leakage assays were carried out to assess the pH-dependent membrane interaction of lipo-OAAs (Figure 3C). The T-shape oligomers with different fatty acids were incubated with erythrocytes at physiological pH 7.4 as well as at endolysosomal pH of 6.5 or 5.5. The results indicate increasing erythrocyte leakage at pH 5.5 with an increasing number of double bonds, which is consistent with previous findings.[40,56] The highest lytic activities were observed for lipo-OAAs containing bis-unsaturated linoleic acid and hydroxy stearic acid. Comparing the lipo-OAA containing SteA and the hydroxylated version of this fatty acid (OHSteA), it is clearly visible that the fatty acid hydroxylation has an enormous effect on the lytic potential. Cis-unsaturated fatty acids are suggested to affect the phase behavior and fluidity of biomembranes,[38,57,58] which explains

https://dx.doi.org/10.1021/acs.bioconjchem.9b00853
Bioconjugate Chem. 2020, 31, 729−742

the higher lytic activity of T-OleA and T-LinA as compared to that of T-SteA.[39] It can be speculated that the bulky hydroxyl group (−HC−OH) in OH-SteA results in a similarly sterically favored angled conformation of hydroxy-stearic acid as compared to constrained cis-unsaturated bonds. The enhanced pH-dependent membrane lysis indicates beneficial effects on cell tolerability at neutral pH and promotes increased endosomal escape due to vesicular acidification.

The advantage of the single hydroxy group in T-OHSteA for triggering endosomal release was further evaluated in endosomal calcein release assays (Figure 3D and E). Neuro2A cells were incubated with calcein for 4 h together in HBG buffer, 75 nM bare RNPs, as well as RNP T-SteA or T-OHSteA nanoparticles. The release of fluorescent calcein from the endosomes into the cytosol was imaged using CLSM (Figure 3D) and quantified by digital image processing (Figure S4). A strong endosomal calcein accumulation was observed in all cases. The bare RNP treated cells did not significantly increase the cytosolic mean fluorescence intensity (CMFI) as compared to HBG treated cells (HBG 2.1 ± 1.7, bare RNPs 5.3 ± 3.1). In contrast, both lipo-OAA formulations increased the CMFI with T-OHSteA mediating the strongest endosomal calcein release (RNP T-SteA 11.2 ± 3.1, RNP T-OHSteA 21.2 ± 4.6). These CLSM results are in line with the quantification of cellular calcein fluorescence by flow cytometry (Figure 3E).

Because the Cas9/sgRNA RNPs have to enter the nucleus after successful endosomal escape, the nuclear association of Cas9-ATTO647N and sgRNA-Cy3 was quantified by performing flow cytometry on isolated nuclei after 24 h of treatment (Figure 3F). Remarkably, even in the case of bare RNPs, a nuclear association of Cas9 was observed. As the cellular uptake experiments also suggested internalization of the bare Cas9 (Figure 3A and B), it seems that the positively charged protein has the ability to enter the cells and reach the nucleus, to some extent. However, neither the uptake (Figure 3A) nor the nuclear association studies suggested successful entry of sgRNA without lipo-OAA formulation. In contrast, cells treated with RNP lipo-OAA nanoparticles exhibited substantial nuclear association of both Cas9 and sgRNA. Consistent with the higher endosomal release, T-OHSteA also mediated the highest nuclear association of sgRNA. To sum, the higher gene knock out efficiency of the RNP T-OHSteA formulation is due to the combination of a number of effects including a more defined particle formation (smallest *z*-average, lowest PDI), enhanced cellular uptake, improved endosomal escape, and in consequence a higher nuclear delivery.

RNP Formulation Variation. GFP knock out efficiency studies (Figure 1) as well as the cellular internalization, endosomal release, and nuclear association experiments (Figure 3) identified the lipo-OAA T-OHSteA as the best performing structure in terms of RNP delivery. To further characterize RNP complex formulation and the optimal composition, dose-titration experiments with varying RNP complex concentrations, varied Cas9 protein to sgRNA molar ratios, as well as varied lipo-OAA nitrogen to sgRNA phosphate (N/P) ratios were performed in two reporter cell lines (Figure 4).

First, nanoparticles were formed at a fixed N/P ratio of 24. The concentration of the RNP complexes in Neuro2a eGFP-Luc and HeLa GFP-Tub treatments ranged from 1 to 100 nM. RNP composition ratios of Cas9 protein to sgGFP of 1:1 (green line) and 1:2 (blue line) were applied (Figure 4A and B). In treatments of Neuro2a eGFP-Luc cells with Cas9/sgRNA RNPs at a ratio of 1:1, the GFP knock out efficiency increased with RNP concentration between 1 and 75 nM and did not improve further at the higher concentration of 100 nM (Figure 4A). In the case of particles containing Cas9:sgGFP RNPs at a ratio of 1:2, the treatment with 50 nM RNP complex mediated the highest GFP knock out efficiency levels, suggesting it as the optimal concentration. Overall, differences between the Cas9/sgRNA composition ratios 1:1 or 1:2 were minor in treatments of Neuro2a eGFP-Luc cells. In contrast, treatments of HeLa GFP-Tub reporter cells resulted in a slightly different observation (Figure 4B); at both ratios, the GFP knock out efficiency increases with increasing RNP concentration up to 50 nM; maximal knock out levels were reached at 50 nM with RNPs at a 1:1 ratio and already at 25 nM with RNPs at a 1:2 ratio. While the knock out efficiency with Cas9/sgGFP RNPs at a 1:1 ratio did not decrease dramatically at higher concentrations, at the 1:2 ratio, it dropped to low levels for concentrations >50 nM of RNPs. The abrupt decrease of the GFP knock out efficiency could be attributed to an increased toxicity due to the double lipo-OAA concentration in the case of RNPs at the 1:2 ratio (Figure S5). Overall, single treatments of HeLa GFP-Tub cells with both Cas9/sgGFP T-OHSteA formulations resulted in remarkably high GFP knock out levels of over 89%. However, it has to be mentioned that the GFP fusion to tubulin in HeLa GFP-Tub cells could negatively affect proliferation, which, in turn, could favor the growth of knock out populations.

Additionally, nanoparticles were formed at different N/P ratios (Figure 4C and D). Two different lipo-OAA concentrations were kept constant, and the RNP levels were gradually increased. On Neuro2a eGFP-Luc cells, lipo-OAA concentrations of 9.5 μM (red line) and 14.3 μM (black line, Figure 4C) were used. GFP knock out efficiencies could be steadily improved by decreasing the N/P ratio with a maximal effect at an N/P ratio of 24 for both concentrations (indicated by the arrows). Because of the higher overall GFP knock out levels on HeLa GFP-Tub cells (Figure 4B), lower lipo-OAA concentrations of 4.8 μM (blue line) and 9.5 μM (red line, Figure 4D) were chosen for this cell line. At a concentration of 4.8 μM lipo-OAA, the successive addition of RNP complexes resulting in N/P ratios of 12 increased GFP knock out levels. At lower N/P ratios, the knock out efficiency dropped, indicating the requirement for an optimal lipo-OAA ratio. At 9.5 μM, the transfection efficiency increased steadily to an N/P ratio of 24, where a plateau was reached. On the basis of these observations, an N/P ratio of 24 in Cas9/sgRNA T-OHSteA complexes was considered optimal.

To assess the RNP delivery potential of T-OHSteA under the determined formulation conditions, the delivery system was compared to other reagents in term of GFP knock out efficiency (Figure 4E). Classical transfection reagents such as succinylated polyethylenimine (PEI-Suc), linear polyethylenimine (linPEI), as well as Lipofectamine CRISPRMAX (LF CM), a commercially available reagent for Cas9/sgRNA RNP transfections, were evaluated in Neuro2a eGFP-Luc cells side-by-side with T-OHSteA. The PEI derivatives were used at published optimal polymer:nucleic ratios (linPEI 0.8 w/w, PEI-Suc 4 w/w).[43] In the case of Lipofectamine, four different procedures (LF CM1−4) with different concentrations and mixing procedures were included for a reliable comparison under the conditions suggested by the manufacturer as well as the parameters of lipo-OAA formulation. The cationizable PEI-polymers, which are known to mediate efficient intracellular

https://dx.doi.org/10.1021/acs.bioconjchem.9b00853
Bioconjugate Chem. 2020, 31, 729−742

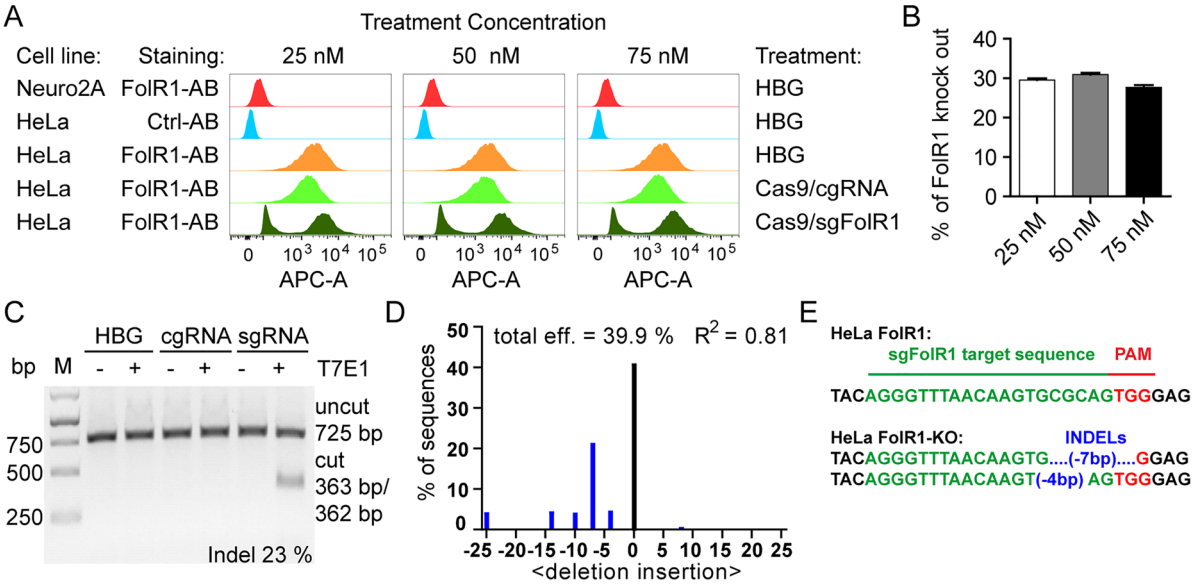

Figure 5. Knock out of the endogenous folate receptor 1 (FolR1). (A) Histograms showing the FolR1 expression of Neuro2a (FolR1 negative cell line) and HeLa (FolR1 positive cell line) cells after 48 h treatment with HBG buffer, Cas9/cgRNA with no specific target in the genome, or Cas9/sgFolR1 targeting the endogenous FolR1 gene. Cells were treated with three different RNP concentrations (25, 50, 75 nM RNPs) complexed with T-OHSteA at an N/P ratio of 24. Read out was performed by flow cytometry 7 d after treatment. For the detection of the folate receptor status, cells were treated with an allophycocyanin (APC)-conjugated antibody against the folate receptor. As a negative control, an APC-conjugated control antibody with no specific target was used. (B) Quantification of the FolR1 knock out efficiency in % as determined by flow cytometry. Cells were normalized to HBG treated cells. Data are presented as mean ± SD (n = 3). (C) The T7E1 assay with FolR1 target region amplicons. Genomic DNA was extracted from HeLa cells treated with HBG buffer, Cas9/cgRNA, or Cas9/sgFolR1 T-OHSteA formulation, and the target region with the sgFolR1 cleavage site in the center was amplified by PCR. After melting and rehybridization, DNA samples were treated with T7E1 and analyzed by agarose gel electrophoresis. The upper bands represent the uncut DNA duplex (725 bp), while the lower band represents the T7E1 cleavage product (362 and 363 bp). The INDEL frequency was estimated by digital quantification of the band intensities (ImageJ). (D) The TIDE analysis[62] of DNA sequences from untreated (control) and Cas9/sgFolR1 T-OHSteA treated HeLa cells. Sanger sequencing data were evaluated by the TIDE web tool (https://tide.deskgen.com/), and an INDEL frequency of 39.9% was determined. (E) Sequencing of monoclonal FolR1 knock out cells. Green sequences indicate the sgRNA target sequence in the FolR1 gene next to the protospacer adjacent motive (PAM) sequence in red. Insertions and deletions (INDELS) caused by the DNA repair mechanisms after the Cas9-induced double-strand break are highlighted in blue.

delivery of nucleic acids such as siRNA and pDNA,[32,43,59] were not able to mediate distinct effects on the GFP expression levels. The cationic lipid Lipofectamine, an otherwise potent transfection reagent, only showed up to 7% GFP knock out at the concentrations and mixing procedures suggested by the manufacturer (LF CM1 and CM2) as well as at the same concentrations used for the RNP T-OHSteA formulations (LF CM3 and CM4). In the side-by-side comparison, the Cas9/sgRNA RNP formulation containing lipo-OAA T-OHSteA outperformed all other reagents, mediating the highest knock out level of 38%.

Successful gene knock out was additionally verified on the genomic level (Figure 4F). After 48 h treatment of Neuro2a, eGFP-Luc cells with 75 nM RNPs complexed with T-OHSteA at an N/P ratio of 24, cells were diluted to generate monoclonal cell populations from single cells. Twenty-nine of the 70 monoclonal cell populations showed a complete loss of GFP expression (determined by flow cytometry), matching the knock out efficiency of previous knock out experiments. The genomic DNA of the cell populations was harvested, and the target region of the GFP gene was amplified by PCR and analyzed by sequencing. Figure 4F illustrates exemplary insertions and deletions (INDELS) at the expected site of the sgGFP target sequence.

Endogenous Gene Knock Out. The Cas9/sgRNA delivery system based on lipo-OAA T-OHSteA demonstrated GFP gene knock out in two artificial reporter cell lines (Figures 1 and 4). To verify that this delivery system can mediate knock out of an endogenous gene, a sgRNA targeting the folate receptor 1 gene (sgFolR1) was loaded into the Cas9-protein and complexed with the carrier system (Figure 5). Lipo-nanoparticles were formed with T-OHSteA and either Cas9/sgFolR1 or Cas9/cgRNA with no specific target in the genome. Folate receptor 1 (FolR1) negative Neuro2a cells and FolR1 positive HeLa cells were incubated with HBG or the RNP-containing delivery systems at 25, 50, and 75 nM (Figure 5A). The FolR1 status upon treatment was assessed by flow cytometry after immunostaining of the cells with an allophycocyanin (APC)-conjugated antibody (FolR1-AB). FolR1 negative Neuro2a cells, which do not express the FolR1, served as a negative control and were not stained with FolR1-AB. As a second negative control for unspecific background fluorescence, FolR1 positive HeLa cells were treated with HBG and subsequently incubated with a control antibody (Ctrl-AB). As a positive control, HeLa cells were treated with HBG and stained with FolR1-AB. At all concentrations, the FolR1 status was clearly positive. Upon incubation of HeLa cells with Cas9/cgRNA, no FolR1 knock out could be detected. In contrast, HeLa cells treated with Cas9/sgRNA showed partial knock out of the endogenous receptor. The FolR1 knock out efficiency of HeLa cells treated with Cas9/sgRNA was quantified (Figure 5B). At all concentrations, FolR1 knock out levels of around 30% were detected.

The knock out of the FolR1 gene was additionally confirmed on the genomic level (Figure 5C–E). Five days after

https://dx.doi.org/10.1021/acs.bioconjchem.9b00853
Bioconjugate Chem. 2020, 31, 729–742

treatment, genomic DNA was extracted, and the target region within the FolR1 gene was amplified by PCR. The amplicons were used to estimate the genome editing rate by using either the T7 endonuclease I assay (T7E1)[60,61] or by the Tracking of Indels by DEcomposition (TIDE)[61,62] analysis of the Sanger sequencing data. The T7E1 assay (Figure 5C) determined an INDEL efficiency of 23% in cells treated with Cas9/sgFolR1 T-OHSteA nanoparticles. In contrast, no INDELS were detected in cells treated with the same formulation containing unspecific cgRNA instead of sgFolR1. The TIDE method compares the Sanger sequencing data of treated and untreated control group DNA. The variety of different INDELS in the treatment group results in a composite sequence trace after the cleavage site. TIDE identifies and quantifies the major induced mutations by a specially developed decomposition algorithm.[62] An interactive web tool (https://tide.deskgen.com/) is available for the convenient and quick assessment of the data (code authored by Eva K. Brinkman, Tao Chen, Mario Amendola, Jos Jonkers, and Bas van Steensel and software authored by Desktop Genetics). The sequencing data of Cas9/sgFolR1 T-OHSteA treated and untreated control cells were analyzed with the TIDE web tool, and a total efficiency of 39.9% of INDELS with a size of up to 25 bp was estimated. The higher INDEL frequency determined by TIDE can be presumably explained by the frequently underestimated mutation frequency determined by the rather semiquantitative T7E1 assay.[61−64] For an exact identification of introduced mutations, cells were diluted to the single cell level 48 h after the treatment. The genomic DNA of the monoclonal cell populations was harvested, and the FolR1 sequences were amplified and analyzed by sequencing. Figure 5E illustrates exemplary INDELS at the expected site of the target sequence.

CONCLUSION

In this study, a novel delivery platform for the delivery of Cas9 protein/sgRNA RNP complexes was developed. Sequence-defined oligo(ethylenamino) amides, which combine the advantages of aminoethylene-based polymers with high chemical precision and flexible design, have been selected and refined for the challenging task. Different lipo-oligomers were used to incorporate the Cas9 protein and different sgRNAs into cationic lipo-OAA nanoparticles. Lipo-OAAs were varied in terms of their fatty acid domains. Structures containing the saturated stearic acid were screened side-by-side to mono- or bis-unsaturated as well as amide-functionalized and hydroxylated lipid moieties. The T-shape lipo-OAA T-OHSteA was identified as the best-performing structure, and the hydroxylation of the contained fatty acid changed the properties and relevant parameters dramatically; the cationic lipo-OAA complexes with Cas9/sgRNA were smaller and more defined and exhibited higher cellular uptake and higher membrane lytic potential. T-OHSteA facilitated efficient intracellular delivery of the RNP complexes and GFP gene knock out efficiencies of up to 40% on Neuro2a eGFP-Luc and up to 89% on HeLa GFP-Tub cells, respectively. In addition, knock out of the endogenous folate receptor 1 gene could be demonstrated in HeLa cells. Overall, the reported lipo-nanoparticles hold great potential for genome editing applications and will be further optimized to target genes for therapeutic applications in vivo.

EXPERIMENTAL PROCEDURES

Materials. Oligoamino amides were synthesized by solid-phase synthesis[30] as described previously.[39] Detailed sequence information can be found in Table S1. HEPES buffered glucose (HBG) containing 20 mM HEPES (Biomol GmbH, Germany) and 5% w/v glucose (Merck, Germany) was adjusted to pH 7.4. ATTO647N NHS-ester was purchased from ATTO-TEC (Germany), and 5-(3-aminoallyl)-uridine-5′-triphosphate-ATTO488 was purchased from Jena Bioscience (Germany). Cell culture media, antibiotics, and fetal bovine serum (FBS) were purchased from Invitrogen (Germany). All solvents and other reagents were purchased from Sigma-Aldrich, Iris Biotech (Germany), Merck (Germany), or AppliChem (Germany). All flasks, dishes, and multiwell plates were manufactured by TPP (Switzerland). Deionized water was purified in-house using an Evoqua Ultra Clear Glass Panel Systems (Germany) and was used for all experiments.

Cas9 Protein Expression and Purification. Recombinant Cas9 was produced by bacterial expression of a plasmid pET28a/Cas9-Cys containing the human codon-optimized Cas9 nuclease gene with a N-terminal His-tag and a C-terminal cysteine. pET28a/Cas9-Cys was a gift from Hyongbum Kim (Addgene plasmid no. 53261; http://n2t.net/addgene:53261; RRID: Addgene_53261).[65] The plasmid pET28a/Cas9-Cys was transformed into RosettaBL21(DE3)pLysS (Merck Millipore, Germany), as recommended by the manufacturer. An overnight culture of RosettaBL21(DE3)plysS (pET28a/Cas9-Cys) was grown in lysogeny broth (LB) medium containing 34 μg/mL chloramphenicol and 50 μg/mL kanamycin at 37 °C under constant shaking. On the next day, the bacterial culture was diluted 1:100 with LB medium (34 μg/mL chloramphenicol and 50 μg/mL kanamycin) and incubated at 37 °C under constant shaking until an optical density of 0.5−0.7 (600 nm) was reached. Afterward, the bacterial suspension was cooled to room temperature (RT), protein expression was induced by adding 1 mM isopropyl β-D-1-thiogalactopyranoside (IPTG), and the culture was incubated overnight at RT under constant shaking. Bacteria were harvested by centrifugation (20 min, 5000*g*, 4 °C). The supernatant was discarded, and the pellet was resuspended in bacterial lysis buffer (20 mM trizma-base, 0.2 M NaCl, 20% sucrose, 10 mM $MgCl_2$, pH 7.5). The final concentrations added were 10 μg/mL RNase, 30 μg/mL DNase, 1 mg/mL lysozyme, and 1 mM phenylmethylsulfonylfluorid (PMSF). The lysed bacterial suspension was frozen in liquid nitrogen, thawed on ice, and sonicated (3 × 20 s on ice). The bacterial lysate was ultracentrifuged (1 h, 20.000 rpm, 4 °C) and filtered using a 0.45 μm syringe filter.

The Cas9 protein was purified by nickel chromatography (HisTrap HP column, GE Healthcare, Sweden) using a gradient from binding buffer (20 mM trizma-base, 0.5 M NaCl, pH 7.4, 20 mM imidazole) to elution buffer (20 mM trizma-base, 0.5 M NaCl, pH 7.4, 0.5 M imidazole). Afterward, the Cas9-containing fractions were concentrated with Amicon Ultra centrifugal filter units (MWCO = 100 kDa, Millipore, U.S.). Finally, the protein solution was subjected to size exclusion chromatography (SEC) using an Äkta purifier system based on a P-900 solvent pump module, a UV-900 spectrophotometrical detector, a pH/C-900 conductivity module, a Frac-950 automated fractionator, and a Superdex 200 size exclusion column using storage buffer (20 mM

https://dx.doi.org/10.1021/acs.bioconjchem.9b00853
Bioconjugate Chem. 2020, 31, 729−742

HEPES, 200 mM KCl, 10 mM $MgCl_2$, and 1 mM DTT) as the solvent. The pooled fractions containing the Cas9 protein were combined, and the amount of purified protein was quantified using a Nanodrop photometer (Thermo Scientific, U.S.) using an extinction coefficient of $\varepsilon/1.000 = 120\ M^{-1}\ cm^{-1}$. The solution was snap-frozen and stored at −80 °C. Protein purity was analyzed on a Coomassie Brilliant Blue stained 10% SDS-PAGE gel (Figure S1).

ATTO647N-Labeling of Cas9 Protein. Cas9 protein was diluted in HEPES (adjusted to pH 8.0 with 0.2 M sodium bicarbonate solution) to a concentration of 2 mg/mL. ATTO647N NHS-ester was solubilized in DMSO (10 mM), and a 2-fold molar excess of reactive dye was added to the protein solution. The mixture was incubated under constant stirring for 1 h at RT. Uncoupled dye was removed by size exclusion chromatography (Äkta purifier system GE Healthcare Bio-Sciences AB, Sweden) with a Superdex 200 size exclusion column using storage buffer (20 mM HEPES, 200 mM KCl, 10 mM $MgCl_2$, 1 mM DTT) as the mobile phase. The pooled fractions containing the Cas9 protein were combined, and the amount of purified protein was quantified using a Nanodrop photometer (Thermo Scientific, U.S.) with an extinction coefficient of $\varepsilon/1.000 = 120\ M^{-1}\ cm^{-1}$. The solution was snap-frozen and stored at −80 °C.

In Vitro Transcription of sgRNAs. The general sgRNA design was based on Larson et al.[66] Specific sgRNA sequences were derived from Qi et al. (sgGFP)[67] and Sun et al. (cgRNA).[20] The DNA template for the in vitro transcription of sgRNA was assembled from two single-stranded oligonucleotides with 21 nucleotide overhangs, which were annealed and extended with T4 DNA polymerase (NEB, Germany). Sequences of the ssDNA oligonucleotides and sgRNAs can be found in Supporting Information section 1.2. The template was purified using a QIAquick PCR Purification Kit (QIAGEN, Germany) and stored in RNase-free water. The linear DNA fragments containing the T7 promoter followed by the sgRNA sequence were analyzed on an agarose gel and transcribed in vitro using the HiScribe T7 High Yield RNA Synthesis Kit (NEB, Germany) according to the manufacturer's instructions. ATTO488-labeled sgRNA was synthesized by substitution of 7% of the UTPs with aminoallyl-UTP-ATTO488 (Jena Bioscience, Germany) during in vitro transcription.

After transcription, 1 μL of DNase was added and incubated for 15 min at 37 °C. The in vitro transcribed sgRNA was purified using the peqGOLD Mikro RNA kit (peqLab, Germany) according to the manufacturer's instructions. The purified sgRNA was heated to 80 °C for 2 min, directly snap-frozen in liquid nitrogen, and stored at −80 °C. Purity of the sgRNA was analyzed on a Gel Red stained 10% DNA-PAGE gel (Figure S1).

In Vitro Cleavage Assay To Test the Functionality of RNPs. To confirm the functionality of Cas9 and sgRNA in vitro, 300 ng of a linearized plasmid or PCR amplicon containing the sgRNA target site was generated. The linear DNA fragment was then incubated with the precomplexed RNPs (150 ng of Cas9 protein and 60 ng of sgRNA) for 2 h at 37 °C. The reaction mixture was analyzed by agarose gel electrophoresis (1.5% agarose gel). Because of the asymmetric location of the sgRNA-target sequence within the amplicon, successful cleavage by the Cas9/sgRNA complex results in two bands on the agarose gel (Figure S1).

Cell Culture. Neuro2a eGFP-Luc, HeLa eGFP-Tub, and HeLa pLuc/705 cells were grown in DMEM medium supplemented with 10% FBS, 100 U/mL penicillin, and 100 μg/mL streptomycin. The cells were cultured in ventilated flasks in the cell incubator at 37 °C and 5% CO_2 in a humidified atmosphere. Cells were passaged at approximately 80% confluency.

Formulation of RNP Oligomer Complexes. To formulate RNP oligomer complexes, the indicated amounts of Cas9 protein and sgRNA were mixed and preincubated for 15 min at RT. For the uptake studies, 20% of the Cas9 protein was substituted by ATTO647N-Cas9 and 20% of the sgRNA by ATTO488-sgRNA. The calculated amount of oligomer at the indicated lipo-nanoparticle (N/P) ratio was diluted in a separate tube (total volume 10 μL) in HBG buffer. After 15 min of incubation of Cas9 and sgRNA, the RNP complex solution is diluted to a volume of 10 μL and added to the oligomer solution, mixed by pipetting, and incubated for another 15 min at RT.

Cellular Treatments under Serum-Free Conditions. For an initial library screening, 5.000 Neuro2a eGFP-Luc cells per well were seeded into 96-well plates the day before cell treatment. Fifteen minutes prior to the treatment, the full serum medium (DMEM containing 10% FBS) was substituted with 80 μL of fresh prewarmed serum-free medium. Twenty microliters of the RNP oligomer complexes formed as described above was added to each well. After 4 h of serum free incubation, 100 μL of medium containing 20% serum was added, and the cells were incubated for another 44 h. After 48 h total incubation time, the cells were transferred into 24-well plates and incubated for additional 72 h. All treatments were performed in triplicate. The knock out efficiency was determined by flow cytometry as the percentage of GFP negative cells after subtraction of unspecific GFP negative population in HBG treated cells. Data are presented as the mean value (±SD) of three independent measurements.

Cellular Treatment under Standard Conditions. RNP lipo-nanoparticle treatments were performed in triplicate in 96-well plates. Cells were seeded 24 h prior to transfection (5.000 cells/well). On the next day, the medium was replaced with 80 μL of fresh prewarmed medium containing 10% FBS. The nanoparticles were prepared as described above, and 20 μL of the transfection mix was added. After 48 h of treatment, the cells were transferred into 24-well plates and incubated for an additional 72 h. The knock out efficiency was determined by flow cytometry as the percentage of GFP negative cells after subtraction of the unspecific GFP negative population in HBG treated cells. Data are presented as the mean value (±SD) of three independent measurements. The relative cell number (%) was calculated relative to control wells treated with HBG as $([A]_{test}/[A]_{control}) \times 100\%$. Data are presented as the mean value (±SD).

Particle Size and Zeta Potential. Particle sizes and zeta potentials of Cas9/sgRNA ribonucleoprotein lipo-nanoparticles were determined by dynamic and electrophoretic light scattering in folded capillary cells (DTS 1070) using a Zetasizer Nano ZS (Malvern Instruments, UK). RNP lipo-nanoparticles containing 12.5 μg of Cas9 protein and 2.5 μg of sgRNA at an N/P ratio of 24 were formed in 200 μL of HBG. For size measurements, each sample was measured three times with 13 subruns at RT. For zeta potential measurements, the sample was diluted to 800 μL with 20 mM HEPES pH 7.4

https://dx.doi.org/10.1021/acs.bioconjchem.9b00853
Bioconjugate Chem. 2020, 31, 729−742

buffer and measured three times with 10−15 subruns. Zeta potentials were calculated via the Smoluchowski equation.[68]

Fluorescence (Cross-) Correlation Spectroscopy (FCS/FCCS). The fluorescence correlation spectroscopy and dual-color fluorescence cross-correlation spectroscopy measurements (FCCS) were performed on a home-built microscope as described elsewhere.[69] A pulsed laser diode at 470 nm wavelength (LDH-P-C-470, PicoQuant) was used for excitation of the ATTO488 labeled sgRNA (ATTO488-sgRNA), and a pulsed laser diode at 635 nm (LDH-P-C-635b, PicoQuant) was used for excitation of the ATTO647N labeled Cas9 protein (ATTO647N-Cas9). Laser powers of ∼4.5 μW for both the 470 and the 635 nm lasers were used, measured at the sample with a slide power meter (S170C-Thorlabs). The measurements were performed using a 60× water immersion objective, NA 1.27 (Plan Apo 60 × WI, Nikon). The correlation analyses were performed with our home-written software PIE analysis with Matlab (PAM).[70] PAM is a stand-alone program (MATLAB; The MathWorks GmbH) for integrated and robust analysis of fluorescence ensemble, single-molecule, and imaging data. The FCS data were acquired by recording the photons with a single APD on a time-correlated single-photon-counting card (TCSPC, SPC-150 Becker and Hickl) for a period of 15 min. The FCCS data were acquired by recording the detected photons on two single-photon avalanche photodiodes (SPADs) using two separate but synchronized TCSPC cards for a period of 15 min. Measurements were conducted in HBG buffer to simulate physiological body conditions.

The autocorrelation functions (ACFs) were fit using a single or two-component model with a triplet fraction, assuming a 3D Gaussian focus shape.

$$G(\tau) = \frac{\gamma}{(A_1 + A_2)^2} \cdot \left[\left(A_1 \left(1 + \frac{4D_1 \cdot \tau}{\omega_r^2} \right)^{-1} \cdot \left(1 + \frac{4D_1 \cdot \tau}{\omega_z^2} \right)^{-1/2} \right) + \left(A_2 \left(1 + \frac{4D_2 \cdot \tau}{\omega_r^2} \right)^{-1} \cdot \left(1 + \frac{4D_2 \cdot \tau}{\omega_z^2} \right)^{-1/2} \right) \right] \cdot \left[1 + \frac{T}{1 - T} \cdot e^{\tau/\tau_T} \right]$$

where A is the size-weighted relative amplitude of particles in the observation volume. When quantitative amplitudes are desired to calculate absolute concentrations, the fraction brightness of the different species needs to be incorporated into the analysis.[51] The A_1 fraction refers to the unbound, freely diffusing labeled sgRNA or Cas9 protein, while A_2 corresponds to the RNP complex bound-labeled sgRNA or Cas9 protein. D_1 and D_2 refer to the respective diffusion coefficients of A_1 and A_2, respectively. The time delay of the autocorrelation is represented by τ. ω_r and ω_z are the lateral and axial focus sizes, respectively, defined as the distance from the focus center to the point where the signal intensity has decreased to $1/e^2$ of the maximum. The geometric factor γ is $2^{-3/2}$ for a 3D Gaussian. The triplet dynamics were accounted for by an additional factor, where T is the triplet fraction and τ_T is the triplet time constant. The fitting was used to extract the fraction of freely diffusing versus complex bound ATTO488-sgRNA/ATTO647N-Cas9, in the absence and presence of the T-OHSteA oligomer. The unbound freely diffusing ATTO488-sgRNA and ATTO647N-Cas9 diffusion coefficients D_1 and D_2 were fixed in the fitting to the values of 56.0 and 18.2 $\mu m^2/s$, respectively, which was previously determined by measuring ATTO488-sgRNA and ATTO647N-Cas9 alone, respectively.

EGFP Reporter Gene Knock Out by Flow Cytometry. After the specified treatments, the cells were collected and resuspended in phosphate-buffered saline (PBS) solution containing 10% FBS (FACS buffer). All samples were analyzed by flow cytometry using a LSR Fortessa flow cytometer (Becton, Dickinson and Company Biosciences, Singapore). Shortly before the measurement, 1 ng/μL 4′,6-diamidino-2-phenylindole (DAPI) was added and used to discriminate between viable and dead cells. The cellular fluorescence was assayed by excitation of DAPI at 405 nm and detection of emission at 450 nm. The cellular eGFP expression was assayed by excitation at 488 nm and the detection of emission at 530 nm. Only isolated viable cells were evaluated. Flow cytometry data were analyzed using FlowJo 7.6.5 flow cytometric analysis software by FlowJo, LLC (Becton, Dickinson and Company, U.S.). All experiments were performed in triplicate.

Cellular Uptake by Confocal Laser Scanning Microscopy (CLSM). Neuro2a cells were seeded in 8-well Ibidi μ-slides (Ibidi GmbH, Germany, 15.000 cells/well) in a total volume of 300 μL of medium per well. Cells were incubated at 37 °C and 5% CO_2. On the next day, the medium was replaced with 240 μL of fresh medium. Cas9/sgRNA RNP (20% ATTO647N labeled Cas9, 20% ATTO488 labeled sgRNA) lipo-nanoparticles were mixed in 60 μL of HBG and added to each well, resulting in a final concentration of 75 nM RNP complex. After 4 h, each well was washed twice with 300 μL of PBS followed by 20 min of incubation on ice with 300 μL of PBS containing 500 IU/mL of heparin. The cells were washed twice with 300 μL of PBS and subsequently fixed with 4% paraformaldehyde in PBS (40 min incubation at RT). After fixation, each well was washed twice with 300 μL of PBS, the cell nuclei were stained with DAPI (2 μg/mL), and F-actin was labeled with rhodamine-phalloidin (1 μg/mL). After 20 min incubation time (light protected at RT), the staining mixture was aspirated and replaced with 300 μL of PBS per well. Images were recorded with a Leica-TCS-SP8 confocal laser scanning microscope (CLSM) equipped with a HC PL APO 63× 1.4 objective (Germany). DAPI emission was recorded at 460 nm, ATTO488-sgRNA at 519 nm, rhodamine at 580 nm, and ATTO647N-Cas9 at 665 nm. All images were processed using the LAS X software from Leica.

Cellular Uptake by Flow Cytometry. One day prior to uptake experiments, Neuro2a WT cells were seeded into 24-well plates at a density of 50.000 cells/well. On the next day, the medium in each well was replaced with 400 μL of fresh medium, and 100 μL of ATTO647N-Cas9/ATTO488-sgRNA RNP lipo-nanoparticles (with an N/P ratio of 24) was added to each well resulting in a final concentration of 75 nM RNP complexes. Control experiments were performed with 100 μL of HBG buffer or ATTO647N-Cas9/ATTO488-sgRNA RNP without the addition of lipo-OAA. Cells were incubated for 4 h at 37 °C and 5% CO_2 in a humidified incubator, collected, and resuspended in PBS buffer containing 10% FBS. All samples were analyzed by flow cytometry using a LSR Fortessa flow cytometer (Becton, Dickinson and Company Biosciences, Singapore). Shortly before the measurement, 1 ng/μL 4′,6-diamidino-2-phenylindole (DAPI) was added and used to discriminate between viable and dead cells. The cellular fluorescence was assayed by excitation of DAPI at 405 nm and detection of emission at 450 nm, the excitation of ATTO647N at 640 nm and detection of emission at 670 nm, and the excitation of ATTO488 at 488 nm and detection of emission at 520 nm. Only isolated viable cells were evaluated. Flow

https://dx.doi.org/10.1021/acs.bioconjchem.9b00853
Bioconjugate Chem. 2020, 31, 729−742

cytometry data were analyzed using FlowJo 7.6.5 flow cytometric analysis software by FlowJo, LLC (Ashland, OR). All experiments were performed in triplicate.

Erythrocyte Leakage Assay. EDTA blood was washed with PBS buffer containing 25 mM sodium citrate. The washed erythrocyte suspension was centrifuged, and the pellet was diluted to 5×10^7 erythrocytes per milliliter with PBS (pH 7.4, 6.5, and 5.5). A volume of 75 μL of erythrocyte suspension and 75 μL of oligomer solution (diluted with PBS at the respective pH) was added to each well of a V-bottom 96-well plate (NUNC, Denmark), resulting in the indicated oligomer concentration. The plates were incubated at 37 °C under constant shaking for 1 h. After centrifugation, 100 μL of the supernatant was analyzed for hemoglobin release by monitoring the absorption at 405 nm using a microplate reader (Spectrafluor Plus, Tecan Austria GmbH, Austria). PBS-treated erythrocytes were set to 0%. Erythrocytes treated with 1% (v/v) Triton X-100 (diluted with PBS at the respective pH) served as a positive control and were set to 100%. Data are presented as the mean value (±SD) of four independent measurements.

Calcein Release Assay by CLSM. One day prior to the RNP lipo-nanoparticle addition, 15.000 Neuro2a WT cells per well were seeded in 8-well Ibidi μ-slides (Ibidi GmbH, Planegg/Martinsried, Germany). The cells were incubated for 4 h with 240 μL of DMEM medium containing 10% FBS and 0.5 mg/mL calcein and an additional 60 μL of Cas9/sgRNA RNP lipo-nanoparticles (with an N/P ratio of 24) resulting in a final concentration of 75 nM RNP complex. Afterward, the cells were washed three times with PBS and fixed in 4% PFA solution for 30 min. After fixation, cells were washed with PBS and finally stored in 300 μL of fresh PBS. Images were recorded by confocal laser scanning microscopy with 488 nm laser excitation (TCS-SP8 confocal laser scanning microscope equipped with an HC PL APO 63× 1.4 objective, Leica Microsystems, Germany).

Calcein Release Assay by Flow Cytometry. One day prior to RNP lipo-nanoparticle addition, 50.000 Neuro2a WT cells per well were seeded in 24-well plates in a total volume of 1 mL per well. The cells were incubated for 4 h with 400 μL of DMEM medium containing 10% FBS and 0.5 mg/mL calcein and an additional 100 μL of Cas9/sgRNA RNP lipo-nanoparticles (with an N/P ratio of 24), resulting in a final concentration of 75 nM RNP complexes. Cells were incubated at 37 °C and 5% CO_2 in a humidified incubator, washed three times with PBS, collected, and resuspended in PBS buffer containing 10% FBS. All samples were analyzed by flow cytometry using a CytoFLEX S flow cytometer (Beckman Coulter, U.S.). Shortly before the measurement, 1 ng/μL 4′,6-diamidino-2-phenylindole (DAPI) was added. Calcein was excited at 488 nm, and emission was detected at 525 nm. Flow cytometry data were analyzed using FlowJo 7.6.5 flow cytometric analysis software by FlowJo, LLC (Ashland, OR). All experiments were performed in triplicate.

Nuclear Association Assay. Neuro2a WT cells (50.000 per well) were seeded into a 24-well plate and incubated for 24 h at 37 °C and 5% CO_2. The medium was replaced with 400 μL of fresh medium, and 100 μL of Cas9-ATTO647N/sgRNA-Cy3 RNP lipo-nanoparticles (with an N/P ratio of 24) were added to each well, resulting in a final concentration of 75 nM RNP complexes. After 24 h, cells were pelleted by centrifugation at 2000g and 4 °C for 10 min. The cells were resuspended in 2 mL of ice-cold phosphate-buffered saline (PBS) containing 2 mM DTT, SIGMAFAST Protease Inhibitor (Sigma-Aldrich, 1 tablet per 100 mL), and 40 μg/mL digitonin. The cells were incubated on ice for 5 min to permeabilize the cells. Subsequently, the nuclei were pelleted by centrifugation at 5000g and 4 °C for 10 min. Nuclei were resuspended in 2 mL of ice-cold phosphate-buffered saline (PBS) containing 2 mM DTT and SIGMAFAST Protease Inhibitor and incubated on ice for 5 min. Nuclei were again pelleted as described above and resuspended in 500 μL of PBS containing 10% FCS for flow cytometry analysis with a CytoFLEX S flow cytometer (Beckman Coulter, U.S.). Shortly before the measurement, 1 ng/μL 4′,6-diamidino-2-phenylindole (DAPI) was added. The nuclei fluorescence was assayed by excitation of DAPI at 405 nm and detection of emission at 450 nm; ATTO647N was excited at 640 nm and emission detected at 670 nm; Cy3 was excited at 561 nm and emission detected at 585 nm. Only isolated nuclei were evaluated. Flow cytometry data were analyzed using FlowJo 7.6.5 flow cytometric analysis software by FlowJo, LLC (Ashland, OR, U.S.). All experiments were performed in triplicate.

Folate Receptor Expression Levels. To examine the folate receptor (FolR1) expression of the different cell lines, 500.000 cells were collected in 100 μL of FACS buffer. For the detection of the FolR1, 5 μL of allophycocyanin (APC)-conjugated α-FolR1 IgG_1 antibody was added and incubated on ice for 1 h. As a negative control, an allophycocyanin (APC)-conjugated anticontrol IgG1 antibody with no specific target was used. After the incubation on ice, cells were washed twice with 1 mL of FACS buffer, resuspended in 600 μL of FACS buffer, and analyzed by flow cytometry using a LSR Fortessa flow cytometer (BD Biosciences, Singapore). Shortly before the measurement, 1 ng/μL DAPI was added and used to discriminate between viable and dead cells. The amount of folic acid receptor positive cells was analyzed through excitation of allophycocyanin at 640 nm and detection of emission at 670 nm. Flow cytometry data were analyzed using FlowJo 7.6.5 flow cytometric analysis software by FlowJo, LLC (Becton, Dickinson and Company, U.S.).

DNA Sequencing. Single cell clones were generated from treated cells as described above using the limiting dilution method in 96-well plates. Genomic DNA of the isolated single cell clones was extracted by a QIAamp DNA Mini Kit (QIAGEN, Germany) following the manufacturer's protocol. The target regions of eGFP or the FolR1 gene were amplified with One*Taq* DNA polymerase (NEB, Germany) using the primers eGFP-F/eGFP-R or FolR1-F/FolR1-R (see the Supporting Information). The amplicons were purified by gel extraction with a QIAquick Gel Extraction Kit (QIAGEN, Germany). Purified amplicons at concentrations of 10−30 ng/μL were sequenced by Eurofins GATC Biotech (Germany) with the primer eGFP-S or FolR1-R. Sequences of the primers can be found in the Supporting Information.

TIDE Analysis. The targeted genomic locus of Cas9/sgFolR1 in HeLa pLuc/705 cells treated and untreated with RNP lipo-nanoparticles was PCR amplified and purified as described above. Sanger sequencing of the purified DNA was performed by Eurofins GATC Biotech (Germany) with the primer FolR1-R (Supporting Information). The raw sequence chromatograms were analyzed by TIDE (Tracking Indels by Decomposition) analysis[62] using the TIDE webtool (https://tide.deskgen.com/), with code authored by Eva K. Brinkman, Tao Chen, Mario Amendola, Jos Jonkers, and Bas van Steensel and software authored by Desktop Genetics. The INDEL size

https://dx.doi.org/10.1021/acs.bioconjchem.9b00853
Bioconjugate Chem. 2020, 31, 729−742

range was set to 25 bp. The sequence segment used for decomposition (decomposition window) was set from 199 bp to 500 bp. The default values for the remaining parameters were used.

T7E1 Assay. Genomic DNA of HeLa pLuc/705 cells was extracted 5 days after treatment using a QIAamp DNA Mini Kit (QIAGEN, Germany) according to the manufacturer's protocol. The target region of the FolR1 gene was amplified with OneTaq DNA polymerase (NEB, Germany) using the FolR1-F/FolR1-R primers (see the Supporting Information). The amplicons were purified by gel extraction with the QIAquick Gel Extraction Kit (QIAGEN, Germany). Purified amplicons (200 ng) were mixed with 2 μL of NEBuffer 2 and nuclease-free water to obtain a total of 19 μL of DNA solution. The reaction was heated to 95 °C for 5 min and then slowly cooled to 25 °C. Afterward, 1 μL of T7 Endonuclease I (NEB, M0302) or nuclease-free water was added to the annealed amplicons and incubated at 37 °C for 30 min. The reaction was stopped by adding 1.5 μL of 0.25 M EDTA solution. The amplicons and cleaved bands were analyzed by agarose gel electrophoresis (2% agarose gel). The fraction of the amplicons cleaved (f_{cut}) was calculated by using ImageJ and the following formula:[60]

$$f_{cut} = \frac{(b + c)}{(a + b + c)}$$

where a is the intensity of the undigested amplicons and b and c are the intensities of cleaved bands. INDEL efficiency was then estimated using the following formula:[60]

$$\text{INDEL}\ (\%) = 100 \times [1 - \sqrt{(1 - f_{cut})}]$$

Statistical Analysis. Data were analyzed with GraphPad prism 5. The statistical significance of the experiments was estimated using the two-tailed student's t test, $^{***}p \leq 0.001$, $^{**}p \leq 0.01$, and $^{*}p \leq 0.05$.

■ ASSOCIATED CONTENT

Supporting Information

The Supporting Information is available free of charge at https://pubs.acs.org/doi/10.1021/acs.bioconjchem.9b00853.

Materials and methods, supporting figures, and analytical data (PDF)

■ AUTHOR INFORMATION

Corresponding Author

Ulrich Lächelt − *Department of Pharmacy and Center for NanoScience (CeNS), Ludwig-Maximilians-Universität München, Munich 81377, Germany;* orcid.org/0000-0002-4996-7592; Phone: +49 89 2180 77842; Email: ulrich.laechelt@lmu.de

Authors

Jasmin Kuhn − *Department of Pharmacy, Ludwig-Maximilians-Universität München, Munich 81377, Germany*

Yi Lin − *Department of Pharmacy, Ludwig-Maximilians-Universität München, Munich 81377, Germany*

Ana Krhac Levacic − *Department of Pharmacy, Ludwig-Maximilians-Universität München, Munich 81377, Germany*

Nader Al Danaf − *Department of Chemistry, Ludwig-Maximilians-Universität München, Munich 81377, Germany*

Lun Peng − *Department of Pharmacy, Ludwig-Maximilians-Universität München, Munich 81377, Germany;* orcid.org/0000-0002-0564-402X

Miriam Höhn − *Department of Pharmacy, Ludwig-Maximilians-Universität München, Munich 81377, Germany*

Don C. Lamb − *Department of Chemistry, Center for NanoScience (CeNS), and Center for Integrated Protein Science Munich (CIPSM), Ludwig-Maximilians-Universität München, Munich 81377, Germany; Nanosystems Initiative Munich (NIM), Munich 80799, Germany;* orcid.org/0000-0002-0232-1903

Ernst Wagner − *Department of Pharmacy and Center for NanoScience (CeNS), Ludwig-Maximilians-Universität München, Munich 81377, Germany; Nanosystems Initiative Munich (NIM), Munich 80799, Germany;* orcid.org/0000-0001-8413-0934

Complete contact information is available at: https://pubs.acs.org/10.1021/acs.bioconjchem.9b00853

Notes

The authors declare no competing financial interest.

■ ACKNOWLEDGMENTS

We thank Olga Brück and Wolfgang Rödl for technical assistance. This manuscript has resulted from the UPGRADE (Unlocking Precision Gene Therapy) project, that has received funding from the European Union's Horizon 2020 research and innovation programme under grant agreement No 825825. We are grateful for financial support from the Excellence Cluster Nanosystems Initiative Munich (NIM) and the Center for NanoScience Munich (CeNS). Funding from the Deutsche Forschungsgemeinschaft (DFG, German Research Foundation) − Project-ID 201269156 − SFB 1032 (projects B3 to D.C.L. and B4 to E.W.) is greatly appreciated. Y.L. and L.P. appreciate the fellowships of the China Scholarship Council that support their Ph.D. studies at the Ludwig Maximilians-Universität München, Germany. U.L. appreciates the support by the Galenus-Privatstiftung (Vienna, Austria).

■ ABBREVIATIONS

OAA, oligo(ethylenamino) amides; RNP, ribonucleoprotein; SteA, stearic acid; OleA, oleic acid; LinA, linoleic acid; NonOcA, nonanamidooctanoic acid; OHSteA, hydroxystearic acid; Stp, succinyl-tetraethylene pentamine; FolR1, folate receptor 1

■ REFERENCES

(1) Leader, B., Baca, Q. J., and Golan, D. E. (2008) Protein therapeutics: a summary and pharmacological classification. *Nat. Rev. Drug Discovery 7*, 21−39.

(2) Goeddel, D. V., Kleid, D. G., Bolivar, F., Heyneker, H. L., Yansura, D. G., Crea, R., Hirose, T., Kraszewski, A., Itakura, K., and Riggs, A. D. (1979) Expression in Escherichia coli of chemically synthesized genes for human insulin. *Proc. Natl. Acad. Sci. U. S. A. 76*, 106−110.

(3) Carter, P. J. (2011) Introduction to current and future protein therapeutics: A protein engineering perspective. *Exp. Cell Res. 317*, 1261−1269.

(4) Lagassé, H., Alexaki, A., Simhadri, V., Katagiri, N., Jankowski, W., Sauna, Z., and Kimchi-Sarfaty, C. (2017) Recent advances in (therapeutic protein) drug development [version 1; peer review: 2 approved]. *F1000Research 6*, 113.

(5) Usmani, S. S., Bedi, G., Samuel, J. S., Singh, S., Kalra, S., Kumar, P., Ahuja, A. A., Sharma, M., Gautam, A., and Raghava, G. P. S.

(2017) THPdb: Database of FDA-approved peptide and protein therapeutics. *PLoS One 12*, e0181748.
(6) Horvath, P., and Barrangou, R. (2010) CRISPR/Cas, the immune system of bacteria and archaea. *Science 327*, 167−70.
(7) Jinek, M., Chylinski, K., Fonfara, I., Hauer, M., Doudna, J. A., and Charpentier, E. (2012) A programmable dual-RNA-guided DNA endonuclease in adaptive bacterial immunity. *Science 337*, 816−21.
(8) Jiang, W., Bikard, D., Cox, D., Zhang, F., and Marraffini, L. A. (2013) RNA-guided editing of bacterial genomes using CRISPR-Cas systems. *Nat. Biotechnol. 31*, 233−239.
(9) Li, J.-F., Norville, J. E., Aach, J., McCormack, M., Zhang, D., Bush, J., Church, G. M., and Sheen, J. (2013) Multiplex and homologous recombination−mediated genome editing in Arabidopsis and Nicotiana benthamiana using guide RNA and Cas9. *Nat. Biotechnol. 31*, 688−691.
(10) Friedland, A. E., Tzur, Y. B., Esvelt, K. M., Colaiácovo, M. P., Church, G. M., and Calarco, J. A. (2013) Heritable genome editing in C. elegans via a CRISPR-Cas9 system. *Nat. Methods 10*, 741−743.
(11) Cho, S. W., Kim, S., Kim, J. M., and Kim, J. S. (2013) Targeted genome engineering in human cells with the Cas9 RNA-guided endonuclease. *Nat. Biotechnol. 31*, 230−2.
(12) Cong, L., Ran, F. A., Cox, D., Lin, S., Barretto, R., Habib, N., Hsu, P. D., Wu, X., Jiang, W., Marraffini, L. A., et al. (2013) Multiplex Genome Engineering Using CRISPR/Cas Systems. *Science 339*, 819−823.
(13) Lino, C. A., Harper, J. C., Carney, J. P., and Timlin, J. A. (2018) Delivering CRISPR: a review of the challenges and approaches. *Drug Delivery 25*, 1234−1257.
(14) Schumann, K., Lin, S., Boyer, E., Simeonov, D. R., Subramaniam, M., Gate, R. E., Haliburton, G. E., Ye, C. J., Bluestone, J. A., Doudna, J. A., et al. (2015) Generation of knock-in primary human T cells using Cas9 ribonucleoproteins. *Proc. Natl. Acad. Sci. U. S. A. 112*, 10437−10442.
(15) Lächelt, U., and Wagner, E. (2015) Nucleic Acid Therapeutics Using Polyplexes: A Journey of 50 Years (and Beyond). *Chem. Rev. 115*, 11043−11078.
(16) Zhang, P., He, D., Klein, P. M., Liu, X., Röder, R., Döblinger, M., and Wagner, E. (2015) Enhanced Intracellular Protein Transduction by Sequence Defined Tetra-Oleoyl Oligoaminoamides Targeted for Cancer Therapy. *Adv. Funct. Mater. 25*, 6627−6636.
(17) Fu, A., Tang, R., Hardie, J., Farkas, M. E., and Rotello, V. M. (2014) Promises and Pitfalls of Intracellular Delivery of Proteins. *Bioconjugate Chem. 25*, 1602−1608.
(18) Wan, T., Niu, D., Wu, C., Xu, F.-J., Church, G., and Ping, Y. (2019) Material solutions for delivery of CRISPR/Cas-based genome editing tools: Current status and future outlook. *Mater. Today 26*, 40−66.
(19) Ramakrishna, S., Kwaku Dad, A. B., Beloor, J., Gopalappa, R., Lee, S. K., and Kim, H. (2014) Gene disruption by cell-penetrating peptide-mediated delivery of Cas9 protein and guide RNA. *Genome Res. 24*, 1020−1027.
(20) Sun, W., Ji, W., Hall, J. M., Hu, Q., Wang, C., Beisel, C. L., and Gu, Z. (2015) Self-assembled DNA nanoclews for the efficient delivery of CRISPR-Cas9 for genome editing. *Angew. Chem., Int. Ed. 54*, 12029−33.
(21) Mout, R., Ray, M., Yesilbag Tonga, G., Lee, Y.-W., Tay, T., Sasaki, K., and Rotello, V. M. (2017) Direct Cytosolic Delivery of CRISPR/Cas9-Ribonucleoprotein for Efficient Gene Editing. *ACS Nano 11*, 2452−2458.
(22) Lee, K., Conboy, M., Park, H. M., Jiang, F., Kim, H. J., Dewitt, M. A., Mackley, V. A., Chang, K., Rao, A., Skinner, C., et al. (2017) Nanoparticle delivery of Cas9 ribonucleoprotein and donor DNA in vivo induces homology-directed DNA repair. *Nature Biomedical Engineering 1*, 889−901.
(23) Chen, G., Ma, B., Wang, Y., and Gong, S. (2018) A Universal GSH-Responsive Nanoplatform for the Delivery of DNA, mRNA, and Cas9/sgRNA Ribonucleoprotein. *ACS Appl. Mater. Interfaces 10*, 18515−18523.
(24) Yue, H., Zhou, X., Cheng, M., and Xing, D. (2018) Graphene oxide-mediated Cas9/sgRNA delivery for efficient genome editing. *Nanoscale 10*, 1063−1071.
(25) Liu, C., Wan, T., Wang, H., Zhang, S., Ping, Y., and Cheng, Y. (2019) A boronic acid-rich dendrimer with robust and unprecedented efficiency for cytosolic protein delivery and CRISPR-Cas9 gene editing. *Science advances 5*, eaaw8922.
(26) Zhou, W., Cui, H., Ying, L., and Yu, X.-F. (2018) Enhanced Cytosolic Delivery and Release of CRISPR/Cas9 by Black Phosphorus Nanosheets for Genome Editing. *Angew. Chem. 130*, 10425−10429.
(27) Chen, Z., Liu, F., Chen, Y., Liu, J., Wang, X., Chen, A. T., Deng, G., Zhang, H., Liu, J., Hong, Z., et al. (2017) Targeted Delivery of CRISPR/Cas9-Mediated Cancer Gene Therapy via Liposome-Templated Hydrogel Nanoparticles. *Adv. Funct. Mater. 27*, 1703036.
(28) Zuris, J. A., Thompson, D. B., Shu, Y., Guilinger, J. P., Bessen, J. L., Hu, J. H., Maeder, M. L., Joung, J. K., Chen, Z.-Y., and Liu, D. R. (2015) Cationic lipid-mediated delivery of proteins enables efficient protein-based genome editing in vitro and in vivo. *Nat. Biotechnol. 33*, 73−80.
(29) Wang, M., Zuris, J. A., Meng, F., Rees, H., Sun, S., Deng, P., Han, Y., Gao, X., Pouli, D., Wu, Q., et al. (2016) Efficient delivery of genome-editing proteins using bioreducible lipid nanoparticles. *Proc. Natl. Acad. Sci. U. S. A. 113*, 2868−2873.
(30) Schaffert, D., Troiber, C., Salcher, E. E., Fröhlich, T., Martin, I., Badgujar, N., Dohmen, C., Edinger, D., Kläger, R., Maiwald, et al. (2011) Solid-Phase Synthesis of Sequence-Defined T-, i-, and U-Shape Polymers for pDNA and siRNA Delivery. *Angew. Chem., Int. Ed. 50*, 8986−8989.
(31) Truebenbach, I., Kern, S., Loy, D. M., Höhn, M., Gorges, J., Kazmaier, U., and Wagner, E. (2019) Combination Chemotherapy of L1210 Tumors in Mice with Pretubulysin and Methotrexate Lipo-Oligomer Nanoparticles. *Mol. Pharmaceutics 16*, 2405−2417.
(32) Boussif, O., Lezoualc'h, F., Zanta, M. A., Mergny, M. D., Scherman, D., Demeneix, B., and Behr, J. P. (1995) A versatile vector for gene and oligonucleotide transfer into cells in culture and in vivo: polyethylenimine. *Proc. Natl. Acad. Sci. U. S. A. 92*, 7297−301.
(33) Lächelt, U., Kos, P., Mickler, F. M., Herrmann, A., Salcher, E. E., Rödl, W., Badgujar, N., Bräuchle, C., and Wagner, E. (2014) Fine-tuning of proton sponges by precise diaminoethanes and histidines in pDNA polyplexes. *Nanomedicine 10*, 35−44.
(34) He, D., Müller, K., Krhac Levacic, A., Kos, P., Lächelt, U., and Wagner, E. (2016) Combinatorial Optimization of Sequence-Defined Oligo(ethanamino)amides for Folate Receptor-Targeted pDNA and siRNA Delivery. *Bioconjugate Chem. 27*, 647−659.
(35) Schaffert, D., Badgujar, N., and Wagner, E. (2011) Novel Fmoc-polyamino acids for solid-phase synthesis of defined polyamidoamines. *Org. Lett. 13*, 1586−9.
(36) Troiber, C., Edinger, D., Kos, P., Schreiner, L., Kläger, R., Herrmann, A., and Wagner, E. (2013) Stabilizing effect of tyrosine trimers on pDNA and siRNA polyplexes. *Biomaterials 34*, 1624−1633.
(37) Fröhlich, T., Edinger, D., Kläger, R., Troiber, C., Salcher, E., Badgujar, N., Martin, I., Schaffert, D., Cengizeroglu, A., Hadwiger, P., et al. (2012) Structure−activity relationships of siRNA carriers based on sequence-defined oligo (ethane amino) amides. *J. Controlled Release 160*, 532−541.
(38) Shin, M. L., Hansch, G., and Mayer, M. M. (1981) Effect of agents that produce membrane disorder on lysis of erythrocytes by complement. *Proc. Natl. Acad. Sci. U. S. A. 78*, 2522−2525.
(39) Reinhard, S., Zhang, W., and Wagner, E. (2017) Optimized Solid-Phase-Assisted Synthesis of Oleic Acid Containing siRNA Nanocarriers. *ChemMedChem 12*, 1464−1470.
(40) Kuhn, J., Klein, P. M., Al Danaf, N., Nordin, J. Z., Reinhard, S., Loy, D. M., Höhn, M., El Andaloussi, S., Lamb, D. C., Wagner, E., et al. (2019) Supramolecular Assembly of Aminoethylene-Lipopeptide PMO Conjugates into RNA Splice-Switching Nanomicelles. *Adv. Funct. Mater. 29*, 1906432.

https://dx.doi.org/10.1021/acs.bioconjchem.9b00853
Bioconjugate Chem. 2020, 31, 729−742

(41) Scholz, C., Kos, P., and Wagner, E. (2014) Comb-Like Oligoaminoethane Carriers: Change in Topology Improves pDNA Delivery. *Bioconjugate Chem. 25*, 251−261.
(42) Liu, X., Zhang, P., He, D., Rödl, W., Preiss, T., Rädler, J. O., Wagner, E., and Lächelt, U. (2016) pH-Reversible Cationic RNase A Conjugates for Enhanced Cellular Delivery and Tumor Cell Killing. *Biomacromolecules 17*, 173−82.
(43) Zintchenko, A., Philipp, A., Dehshahri, A., and Wagner, E. (2008) Simple modifications of branched PEI lead to highly efficient siRNA carriers with low toxicity. *Bioconjugate Chem. 19*, 1448−55.
(44) Akinc, A., Zumbuehl, A., Goldberg, M., Leshchiner, E. S., Busini, V., Hossain, N., Bacallado, S. A., Nguyen, D. N., Fuller, J., Alvarez, R., et al. (2008) A combinatorial library of lipid-like materials for delivery of RNAi therapeutics. *Nat. Biotechnol. 26*, 561−569.
(45) Semple, S. C., Akinc, A., Chen, J., Sandhu, A. P., Mui, B. L., Cho, C. K., Sah, D. W. Y., Stebbing, D., Crosley, E. J., Yaworski, E., et al. (2010) Rational design of cationic lipids for siRNA delivery. *Nat. Biotechnol. 28*, 172−176.
(46) Albanese, A., Tang, P. S., and Chan, W. C. (2012) The effect of nanoparticle size, shape, and surface chemistry on biological systems. *Annu. Rev. Biomed. Eng. 14*, 1−16.
(47) Lundqvist, M., Stigler, J., Elia, G., Lynch, I., Cedervall, T., and Dawson, K. A. (2008) Nanoparticle size and surface properties determine the protein corona with possible implications for biological impacts. *Proc. Natl. Acad. Sci. U. S. A. 105*, 14265−70.
(48) Huhn, D., Kantner, K., Geidel, C., Brandholt, S., De Cock, I., Soenen, S. J., Rivera Gil, P., Montenegro, J. M., Braeckmans, K., Mullen, K., et al. (2013) Polymer-coated nanoparticles interacting with proteins and cells: focusing on the sign of the net charge. *ACS Nano 7*, 3253−63.
(49) Elson, E. L., and Magde, D. (1974) Fluorescence correlation spectroscopy. I. Conceptual basis and theory. *Biopolymers 13*, 1−27.
(50) Magde, D., Elson, E., and Webb, W. W. (1972) Thermodynamic Fluctuations in a Reacting System—Measurement by Fluorescence Correlation Spectroscopy. *Phys. Rev. Lett. 29*, 705−708.
(51) Ivanchenko, S., Lamb, D. C., Brnjas-Kraljević, J., and Pifat-Mrzljak, G. (2011) *Supramolecular Structure and Function 10* p 1, Springer, Netherlands.
(52) Schwille, P., Meyer-Almes, F. J., and Rigler, R. (1997) Dual-color fluorescence cross-correlation spectroscopy for multicomponent diffusional analysis in solution. *Biophys. J. 72*, 1878−86.
(53) Müller, B. K., Zaychikov, E., Brauchle, C., and Lamb, D. C. (2005) Pulsed interleaved excitation. *Biophys. J. 89*, 3508−22.
(54) Varkouhi, A. K., Scholte, M., Storm, G., and Haisma, H. J. (2011) Endosomal escape pathways for delivery of biologicals. *J. Controlled Release 151*, 220−8.
(55) Lonn, P., Kacsinta, A. D., Cui, X. S., Hamil, A. S., Kaulich, M., Gogoi, K., and Dowdy, S. F. (2016) Enhancing Endosomal Escape for Intracellular Delivery of Macromolecular Biologic Therapeutics. *Sci. Rep. 6*, 32301.
(56) Klein, P. M., Reinhard, S., Lee, D. J., Muller, K., Ponader, D., Hartmann, L., and Wagner, E. (2016) Precise redox-sensitive cleavage sites for improved bioactivity of siRNA lipopolyplexes. *Nanoscale 8*, 18098−18104.
(57) Le Gall, T., Loizeau, D., Picquet, E., Carmoy, N., Yaouanc, J. J., Burel-Deschamps, L., Delepine, P., Giamarchi, P., Jaffres, P. A., Lehn, P., et al. (2010) A novel cationic lipophosphoramide with diunsaturated lipid chains: synthesis, physicochemical properties, and transfection activities. *J. Med. Chem. 53*, 1496−508.
(58) Malamas, A. S., Gujrati, M., Kummitha, C. M., Xu, R., and Lu, Z. R. (2013) Design and evaluation of new pH-sensitive amphiphilic cationic lipids for siRNA delivery. *J. Controlled Release 171*, 296−307.
(59) Zou, S. M., Erbacher, P., Remy, J. S., and Behr, J. P. (2000) Systemic linear polyethylenimine (L-PEI)-mediated gene delivery in the mouse. *J. Gene Med. 2*, 128−34.
(60) Ran, F. A., Hsu, P. D., Wright, J., Agarwala, V., Scott, D. A., and Zhang, F. (2013) Genome engineering using the CRISPR-Cas9 system. *Nat. Protoc. 8*, 2281−2308.
(61) Sentmanat, M. F., Peters, S. T., Florian, C. P., Connelly, J. P., and Pruett-Miller, S. M. (2018) A Survey of Validation Strategies for CRISPR-Cas9 Editing. *Sci. Rep. 8*, 888.
(62) Brinkman, E. K., Chen, T., Amendola, M., and van Steensel, B. (2014) Easy quantitative assessment of genome editing by sequence trace decomposition. *Nucleic Acids Res. 42*, e168−e168.
(63) Kim, J. M., Kim, D., Kim, S., and Kim, J.-S. (2014) Genotyping with CRISPR-Cas-derived RNA-guided endonucleases. *Nat. Commun. 5*, 3157.
(64) Ehrke-Schulz, E., Bergmann, T., Schiwon, M., Doerner, J., Saydaminova, K., Lieber, A., and Ehrhardt, A. (2016) Quantification of designer nuclease induced mutation rates: a direct comparison of different methods. *Mol. Ther.–Methods Clin. Dev. 3*, 16047−16047.
(65) Ramakrishna, S., Kwaku Dad, A.-B., Beloor, J., Gopalappa, R., Lee, S.-K., and Kim, H. (2014) Gene disruption by cell-penetrating peptide-mediated delivery of Cas9 protein and guide RNA. *Genome Res. 24*, 1020−1027.
(66) Larson, M. H., Gilbert, L. A., Wang, X., Lim, W. A., Weissman, J. S., and Qi, L. S. (2013) CRISPR interference (CRISPRi) for sequence-specific control of gene expression. *Nat. Protoc. 8*, 2180−96.
(67) Qi, L. S., Larson, M. H., Gilbert, L. A., Doudna, J. A., Weissman, J. S., Arkin, A. P., and Lim, W. A. (2013) Repurposing CRISPR as an RNA-guided platform for sequence-specific control of gene expression. *Cell 152*, 1173−83.
(68) Smoluchowski, M. V. (1916) Drei Vortrage uber Diffusion, Brownsche Bewegung und Koagulation von Kolloidteilchen. *Z. Phys. 17*, 557−585.
(69) Hendrix, J., Baumgartel, V., Schrimpf, W., Ivanchenko, S., Digman, M. A., Gratton, E., Krausslich, H. G., Müller, B., and Lamb, D. C. (2015) Live-cell observation of cytosolic HIV-1 assembly onset reveals RNA-interacting Gag oligomers. *J. Cell Biol. 210*, 629−46.
(70) Schrimpf, W., Barth, A., Hendrix, J., and Lamb, D. C. (2018) PAM: A Framework for Integrated Analysis of Imaging, Single-Molecule, and Ensemble Fluorescence Data. *Biophys. J. 114*, 1518−1528.

https://dx.doi.org/10.1021/acs.bioconjchem.9b00853
Bioconjugate Chem. 2020, 31, 729−742